Using remote sensing and ground based measurements to identify vegetation-geomorphology patterns in permafrost

GEOQuébec 2015
Challenges from North to South
Des défis du Nord au Sud

Thomas A. Douglas, C.A. Hiemstra & Kevin Bjella
U.S. Army Cold Regions Research and Engineering Laboratory, Fort Wainwright, Alaska, USA
M.T. Jorgenson
Alaska Ecosience, Fairbanks, Alaska, USA
S. Newman & E. Deeb
U.S. Army Cold Regions Research and Engineering Laboratory, Hanover, NH, USA
John Anderson
U.S. Army Geospatial Research Laboratory, Richmond, Virginia, USA

ABSTRACT
Ice content, sediment composition, and vegetation are key variables in predicting how and where permafrost will respond to projected Arctic climate warming. Orbital and suborbital remote sensing tools, historical imagery, pattern detection, and LiDAR can be combined to provide a holistic view of how and where the landscape will respond to climate warming. However, this information can only provide realistic results when it is calibrated with field measurements representing a variety of terrain states, seasonal variations, and physical and chemical processes. This presentation will include remote sensing, field survey, and ground based geophysical measurements from a variety of discontinuous permafrost terrains in interior Alaska. We have combined electrical resistivity tomography, airborne LiDAR, active layer measurements, and high resolution surveying to link landscape features with permafrost ice content, vegetation, and the soil thermal regime.

RÉSUMÉ
La teneur en glace, la composition des sédiments, et la végétation sont des variables clés pour prédire la réponse du pergélisol aux futures projections de réchauffement climatique en région Arctique. Les outils de télédétection orbitaux et suborbitaux, l'imagerie historique, la détection de motifs, et les données LiDAR, peuvent être combinés pour fournir une vue globale de la manière dont le paysage répondra au réchauffement climatique. Cependant, ces informations ne peuvent fournir des résultats réalistes que quand elles sont étalonnées avec des mesures de terrain représentant la variabilité spatiale et saisonnière et la variabilité des processus physiques et chimiques en action. Cette présentation inclura télédétection, arpentage et mesures géophysiques de terrain, obtenues pour une variété de terrains à pergélisol discontinu de l'Alaska Intérieure. Nous avons combiné des données tomographiques de résistivité électrique, des données de LiDAR aéroporté, des mesures de la couche active et des mesures d'arpentage à haute résolution pour relier les caractéristiques du paysage avec la teneur en glace du pergélisol, la végétation, et le régime thermique du sol.

1 INTRODUCTION

Mean annual temperatures in interior Alaska, currently -1°C, are predicted to increase 5°C over the next 80 years (Chapman and Walsh, 2007). This is expected to initiate widespread permafrost degradation which could alter hydrogeology, soils, vegetation, and microbial communities (Racine and Walters, 1994; Walker et al., 2006; Mackelprang et al., 2011; Wilhelm et al., 2011; Wolken et al., 2011; Douglas et al., 2013). Permafrost degradation will provide a challenge for the design and maintenance of vertical and horizontal infrastructure. In addition, carbon cycle processes are likely to change in northern boreal permafrost ecosystems due to alterations in soil, vegetation, and wetland properties (Grosse et al., 2011).

Permafrost stability/instability is controlled by the soil thermal regime which is influenced by soil texture, plant cover, air temperature, snowfall, topography, slope, aspect, hydrology, ground ice content, and fire history (Osterkamp and Romanovsky, 1999; Jorgenson and Osterkamp, 2005; Myers-Smith et al., 2008). Changes in permafrost extent can lead to subsidence and the formation of wetland features like bogs, fens, and muskegs when low lying areas accumulate snow melt and rain water (Smith et al., 2005).

Identifying where and predicting how permafrost will respond to climate warming or disturbance like fire or human development requires accurate assessment of subsurface properties and composition. Permafrost with high ice content is particularly vulnerable to climate warming or disturbance. High ice content permafrost is of particular importance because its' degradation leads to thermokarst which alters the landscape markedly. Where permafrost is associated with surface biophysical characteristics that can be measured remotely, standoff detection tools (suborbital or satellite based measurements and repeat imagery analysis) could be applied toward mapping permafrost and tracking its trajectories of change over large regions. There is a need to apply these types of analyses over large spatial scales to identify permafrost bodies, particularly locations of high ice content, to support engineering, ecological, and hydrologic investigations

Geophysical techniques, predominantly electrical resistivity tomography (ERT), have been recently coupled with airborne or other ground based measurements to identify permafrost extent and associate ice content with terrain geomorphology (Yoshikawa et al., 2006; Douglas et al., 2008; Lewkowicz et al., 2011; Hubbard et al., 2013) and biophysical characteristics (Douglas et al., in press). ERT works well for mapping frozen ground because the electrical resistivity (in Ω–m) of an earth material is drastically different whether it is frozen or thawed (Hauck and Kneisel, 2008). Resistivity (ρ) values of frozen soils can be 10 to 1,000 times greater than unfrozen soils (Harada and Yoshikawa, 1996).

This study mapped permafrost distribution using ERT, thaw probing, airborne LiDAR, snow depth measurements, coring, and thermal measurements to identify relationships between vegetation, permafrost extent, and permafrost ice content. We focused our efforts across 400 to 500 m long transects at an upland and two lowland sites near Fairbanks, Alaska. Specific objectives of the research were to: (1) document vegetation, topography, thaw depths, snow, and terrain elevation across the transects; (2) quantify permafrost distribution with thaw probing and ERT; and (3) relate airborne photographic and LiDAR imagery with permafrost properties.

2 FIELD MEASUREMENTS

2.1 Field locations and site descriptions

Discontinuous permafrost features in interior Alaska are tens of meters thick and are most commonly located in lowlands, on north-facing slopes and where soils or vegetation are suitable for maintaining frozen ground (Racine and Walters, 1994; Chacho et al., 1995; Jorgenson et al., 2008). The area contains ice rich “yedoma-type” permafrost with a carbon content of 2–5% which is up to 30 times greater than thawed mineral soils (Zimov et al., 2006). This Pleistocene syngenetic yedoma permafrost formed through repeated deposition of windblown loess and organic matter (Shur and Jorgenson, 2007). Worldwide, yedoma permafrost is believed to contain almost 1.7 billion metric tons of organic carbon, one quarter of the northern latitude permafrost soil carbon pool (Tarnocai et al., 2009). Interior Alaska permafrost has also been formed from alluvial and aeolian materials (syngenetic), peat accumulation (syngenetic and quasi-syngenetic) and climate variations (epigenetic; Shur and Jorgenson, 2007).

Our field sites included a 400 m long transect through upland terrain above the CRREL Permafrost Tunnel in Fox, Alaska and 500 m long transects in lowlands at both the CRREL Farmer’s Loop Permafrost Experimental Station and the Creamer’s Field migratory Refuge near Fairbanks (Figures 1 and 2). The sites were selected based on their likelihood of having ice features in the subsurface, the variety of ecotypes represented at a given site, ancillary information on the permafrost from previous studies, and access to the road system.

2.2 Satellite and LiDAR imagery

Recent high-resolution satellite multispectral imagery (usually 2 to 4 m resolution) and a companion panchromatic image (~0.5 to 0.6 m) were obtained for all of the sites. Airborne LiDAR imagery was collected from May 9-11, 2014 by Quantum Spatial Incorporated (Anchorage, Alaska). A Leica (Wetzlar, Germany) ALS70 system (1064 nm) mounted in a Partenavia aircraft was acquired imagery at an average pulse density of ≥25 pulses/m^2 and an altitude of 1,000 m. Aircraft position was measured twice per second (2 Hz) by onboard differential geographic positioning system (dGPS). Altitude was measured 200 times per second (200 Hz) as pitch, roll and yaw (heading) from an onboard inertial measurement unit. To allow for post-processing correction and calibration, aircraft and sensor position and attitude data were indexed by GPS time. The measurement accuracy from these measurements yielded a root mean square error (RMS) of ≤9.2 cm and a spatial resolution of 0.25 m.

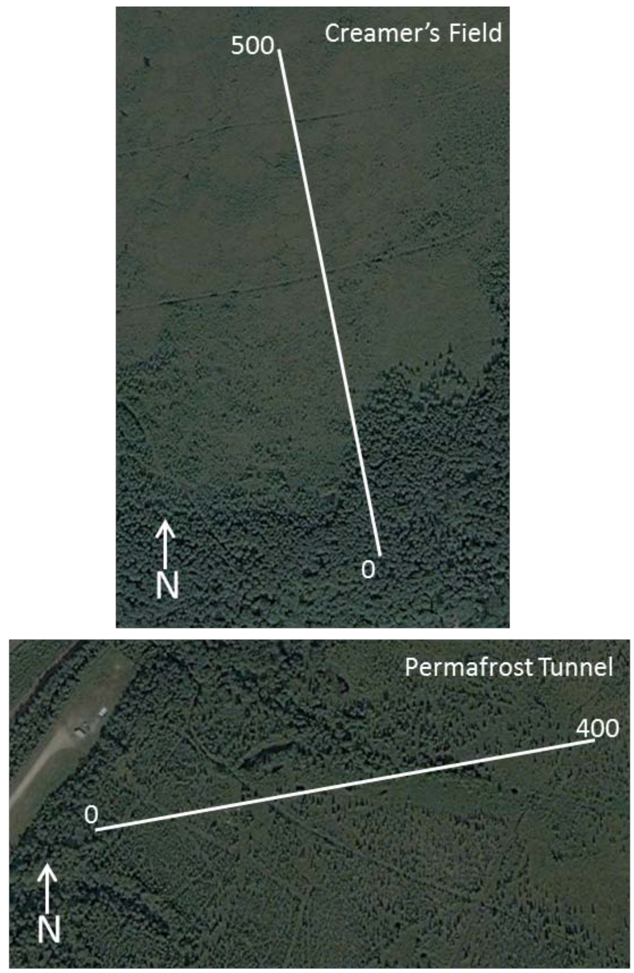

Figure 1. A Google Earth image of the Creamer’s Field and Farmer’s Loop field site transects for this study. The Farmer’s Loop transect is presented in more detail in Figure 2. Transect lengths are given in meters.

2.3 Field survey measurements

In the spring of 2013 the transect end points were surveyed and 1-m wide trails were hand cleared of large woody vegetation to improve access for surveying and geophysical measurements. Five to ten thermistors were installed at each site in locations representing a variety of soil, vegetation, and landscape properties. They were installed roughly 100 m apart. During the winter of 2013-2014 snow pack depths were made at roughly 1 m intervals along the side of each transect line multiple times using a snow depth datalogger coupled with a GPS. Typically, 400 snow depths were made along each transect. During the summer of 2014 maximum seasonal thaw depths were determined repeatedly at 4 m intervals along the side of each transect. Small numbered pinflags were installed at each thaw probe location and their GPS locations were measured. This allowed for the collection of repeat thaw depth measurements at the same exact locations across a given transect to prevent localized soil or vegetation features, particularly tussocks, from affecting thaw depth measurements. We used a 1 cm diameter 1.7 m long graduated metal rod ("frost probe") to make depth measurements of the seasonally thawed "active" layer. The probe was pushed into the ground until refusal to measure the distance between the ground surface and the top of either the winter season freeze layer or the top of permafrost. A Geoprobe 7822 Direct Push Technology track mounted drill rig was used to collect deeper (20 m) cores along the transects. Gravimetric ice content measurements and sediment identifications were made from sections of these cores.

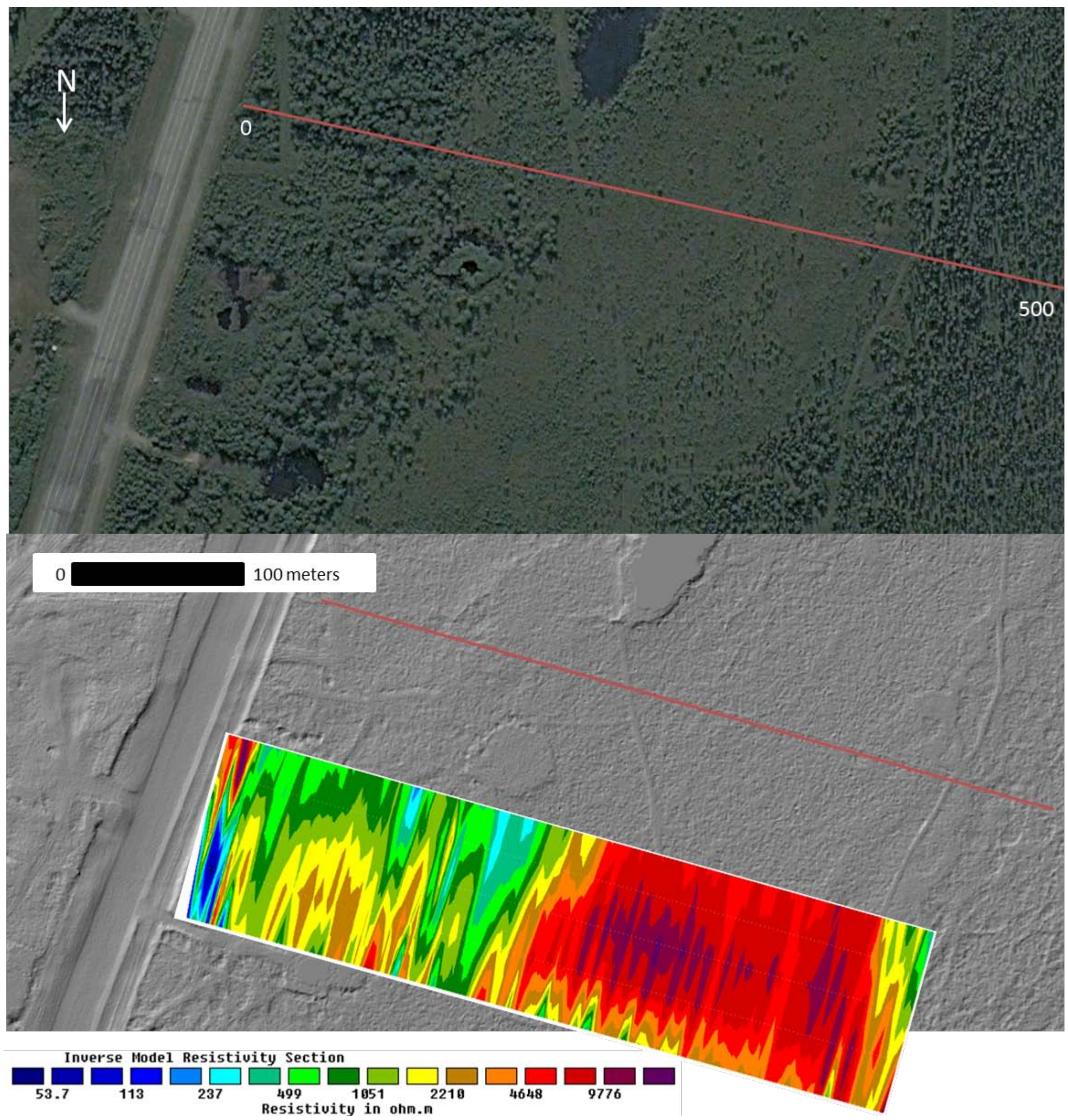

Figure 2. A Google Earth image (top) and airborne LiDAR and the ERT cross section (bottom) from the Farmer's Loop site. Similar measurements were made along a second Farmer's Loop transect and at the Creamer's Field and Permafrost Tunnel transects but the results are not shown here.

2.4 Electrical resistance tomography

Electrical resistance tomography (ERT) measurements were made with an Advanced Geosciences Incorporated (Austin, Texas) "SuperSting" R8 eight channel portable induced polarization galvanic earth resistivity meter. Permafrost resistivity values have been measured in the Fairbanks area in multiple studies. Resistivity values of 800 Ω-m were reported for permafrost at -5°C (Hoekstra and McNeill, 1973). Resistivity values of >600 Ω-m were previously reported at the CRREL Farmer's Loop Permafrost Experimental Station (Douglas et al., 2008), values of 600–10,000 Ω-m were measured at a pingo located 4 km west of the Permafrost Experimental Station (Yoshikawa et al., 2006), and resistivity values of 1,000 to 25,000 were recently measured at five locations in the Tanana Flats lowlands south of Fairbanks (Douglas et al. in press). For the purposes of this study resistivity values of 1,000 Ω-m or greater are deemed indicative of permafrost.

Six cables, each with 14 take-out electrodes, were employed at 2.5 m spacings along the transects to achieve a maximum ERT penetration depth into the subsurface of ~25 m. The electrodes were 45 cm long. The R8 control module was set up between electrodes 42 and 43. A dipole-dipole array was used for all measurements to provide optimal horizontal resolution for detection of vertical structures (Kneisel, 2006). Contact resistance was measured at each electrode until adequate resistance (<2,000 Ω-m) was reported along the 84 electrode line.

Two-dimensional model interpretation was performed using RES2DINV (Geotomo Software, Penang, Malaysia). This software package performs smoothing and constrains inversion using finite difference forward modeling and quasi-Newton techniques (Loke et al., 2003). Employing a least-squares inversion, convergence was tested by comparing the change in RMS quadratic error between multiple iterations until RMS error reached 5% where further iterations would not significantly lower the RMS values.

3 RESULTS AND DISCUSSION

3.1 Satellite and LiDAR imagery

Patterned (polygonal) ground is evident in aerial imagery all along the Creamer's Field transect (Figure 1, top). These features are also evident visually at the ground surface in the mixed birch and spruce forest comprising the first ~150 meters of the transect. However, when the transect transitions from the forest to the tussock and shrub area the ice wedge polygons are no longer evident from the ground surface. There is evidence of ice wedge polygon structures at the Farmer's Loop field site (based on WorldView satellite and LiDAR analysis). Polygonal (patterned) ground is not identifiable in either WorldView or LiDAR imagery at the surface along the Permafrost Tunnel transect. Ice wedges are present throughout the 250 m long subsurface tunnel system, which runs below the transect, but they are covered by a ~5 m thick surface layer of Holocene silt (Hamilton et al., 1988) and a dense surface vegetation cover. Anthropogenic features (i.e. disturbances) like roads, trails, and clearings, are easily identifiable in the satellite and LiDAR imagery at all sites (Figures 1 and 2).

3.2 Field survey measurements

At the Farmer's Loop site the transect begins in a mixed birch and spruce forest (the first ~110 m), then passes through a treed fen (120-200 m), a section of tussock and shrubs (200-420 m), and ends in a thick black spruce forest (420-500 m). Measurements from the Farmer's Loop transect are the main focus here due to space limitations but many of the relationships between permafrost morphology and composition, vegetation, and our airborne and surface measurements are consistent across all three sites. An example of a typical one year soil temperature record with depth is provided as Figure 3. At this location the seasonal thaw depth is roughly 70 cm. Repeat snow depth measurements were made across the transects three times during the winter of 2013-2014 and the results from Farmer's Loop are provided as Figure 4. There is a strong relationship between snow depth, vegetation, and areas of anthropogenic disturbance. Only snow depth measurements from the Farmer's Loop transect are provided here but the relationships we present from the Farmer's Loop site are consistent across all three sites. Snow depths are the lowest in the forested regions. It is likely that snow is captured by the forest and this leads to the lower overall depths throughout the winter.

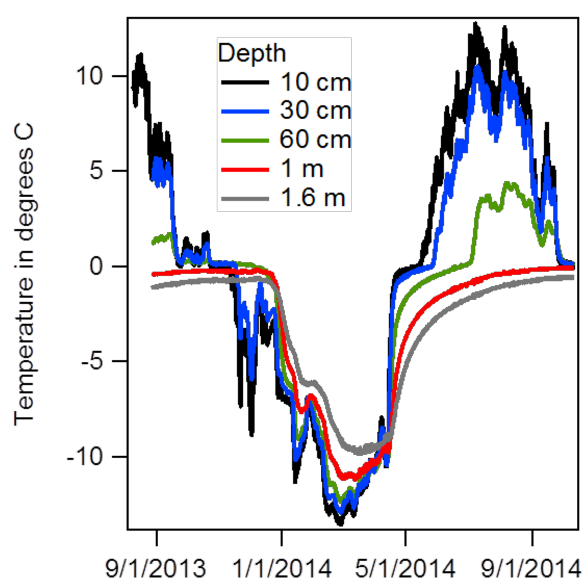

Figure 3. Temperatures by depth measured at the tussock zone of the Farmer's Loop site.

From 200 to 400 m along the Farmer's Loop transect, the area comprised of sedge tussocks and birch and alder shrubs, snow depths are greatest during all three sets of measurements. The extreme heterogeneity of snow depths in this region is dependent on whether the depth measurements were made between tussock tops or on top of the tussock features. The mean tussock height is roughly 40 cm.

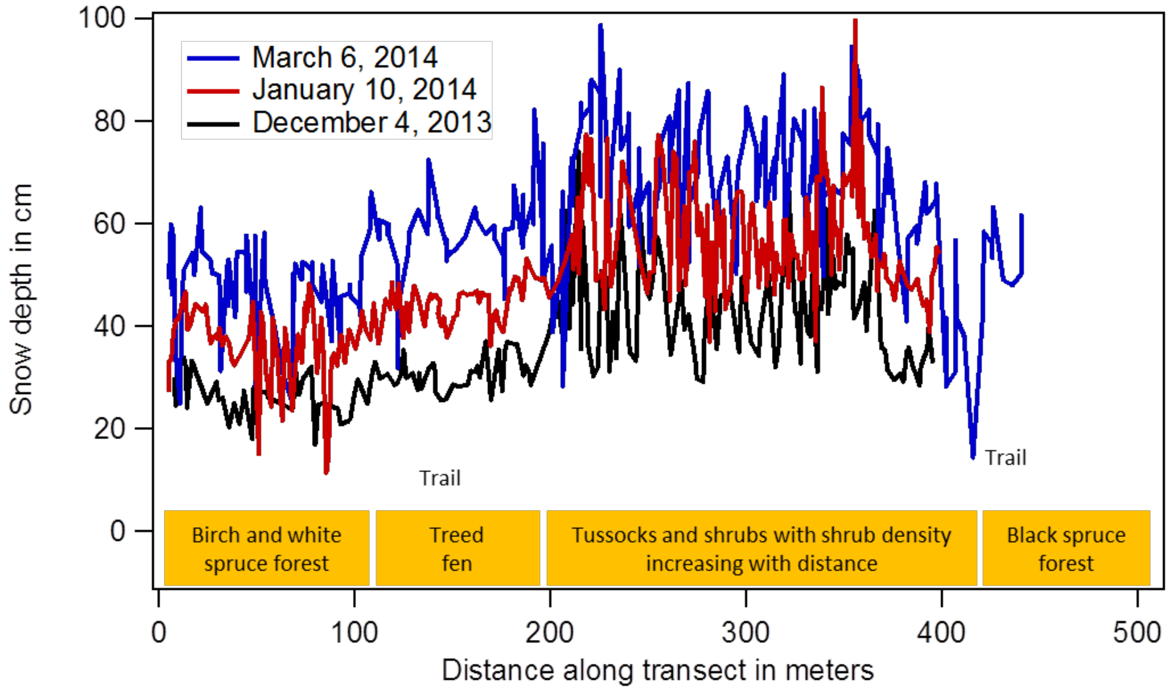

Figure 4. Repeat snow depth measurements across the Farmer's Loop transect. Note the strong relationship between vegetation type/ecotype and snow depth and the low snow depths at the two trail crossings.

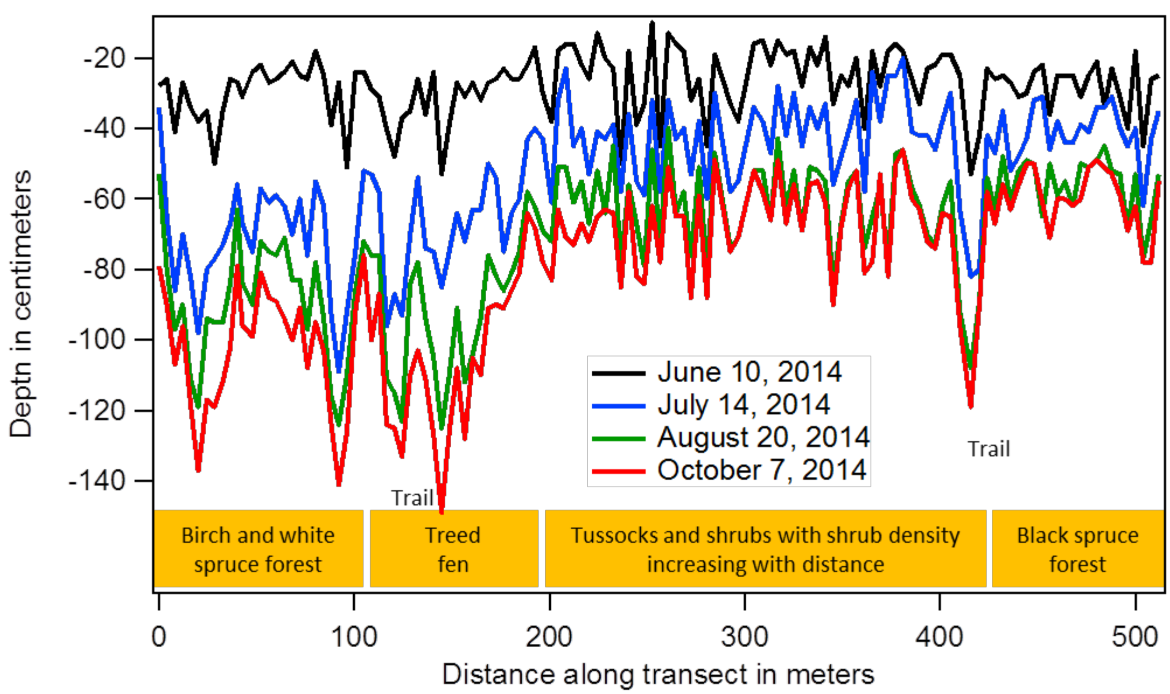

Figure 5. Repeat thaw probe measurements across the Farmer's Loop transect. Note the strong relationship between vegetation type/ecotype and thaw depth and the low markedly deeper thaw at the two trail crossings.

With increasing distance along the tussock zone of the transect the shrub height and density increase while the tussock height and density remain consistent. The denser and taller shrubs likely decrease wind speeds in this area and minimize the movement of blowing snow into or from this area. As such, the deepest snow of the transect is measured in this region. The same relationship between increasing shrub density and height and increasing snow depths is also apparent at the Creamer's Field site (not shown) and supports previous research on snow-vegetation interactions from similar vegetation on the Seward Peninsula of Alaska (Sturm et al., 2005). At the upland Permafrost Tunnel site the vegetation is more consistent across the transect and, as a consequence, the snow pack is more uniform.

Results from repeat seasonal thaw depth measurements (Figure 5) also show a strong relationship with vegetation along the Farmer's Loop transect as well as the other two sites (not shown here). For example, the mixed birch and spruce forest present for the first ~120 m of the transect is associated with the deepest seasonal thaw measurements. The tussock/shrub and spruce forest zones consistently yield the lowest seasonal thaw measurements.

Figure 6. Photographs of cores and water content measurements from the white spruce and birch forest (left) and tussock zones (right) at the Farmer's Loop site. The scales are in decimal feet (each major marker is ~2.5 cm).

Roughly 60% of the seasonal thaw along the transects occurred by mid-July and downward movement of the thaw front had mostly ceased by late August with little additional thaw between August 20 and early October. The shrub and spruce forested regions of the transect underwent minimal to no changes in seasonal thaw from August 20 to early October while the mixed birch and spruce forest and the treed fen added roughly 10 cm of additional thaw. Disturbances, like the two ski trails along the Farmer's Loop transect and similar trails at the Creamer's Field and Permafrost Tunnel sites, are associated with dramatically deeper seasonal thaw. Removal or alteration of the organic soil layer or moss ground cover increases the ground heat flux and promotes more rapid seasonal and permafrost thaw (Nicholas and Hinkel, 1996) and loss of the "ecosystem protection" of permafrost in the area (Shur and Jorgenson, 2007).

Figure 6 includes photographs and water content information from cores collected along the Farmer's Loop transect. A total of nine ~30 m long cores were collected from the site and the core locations represented the variety of ecotypes present. Cores collected at the Creamer's Field site, where both mixed forest and tussock regions are present, yielded similar results. Cores from the permafrost tunnel site generally yielded low water contents (50-200 g/g) and no peat layers.

3.3 Electrical resistance tomography

All of our transects are underlain by permafrost across the entire transect but differences in ERT resistivity measurements are linked to changes in ice content. For example, at the Farmer's Loop transect the birch and white spruce forest and the black spruce forest are underlain by silts with minor peat and low ice contents of 30 to 100 g/g (Figure 6). These areas yielded ERT ρ values of 800 to 1,500 Ω-m. There is a dramatic shift toward increased ρ values ~210 m into the transect (>4,000 Ω-m , Figure 2). This corresponds with the region of tussocks and shrub vegetation and ice rich peats (Figure 6m right) in the subsurface. ERT results from the Creamer's Field site show a similar relationship between increased ρ values and ice content. The areas with elevated ERT ρ values are associated with higher ice content permafrost and decreased seasonal thaw depths.

At the permafrost tunnel site the ERT ρ values are 1,000 to 2,000 Ω-m in the upper ~4 m with a repeating pattern of markedly higher ρ values (5,000 to 10,000 Ω-m) from 4 to 10 m in depth and at a ~10 m spacing (not shown). We interpret these high resistivity value areas to represent ice wedge polygon structures in the subsurface, likely the "Upper Silt Unit" overlain by Holocene silts as mapped by Hamilton et al. (1988) and corroborated by our core drilling at the site. These subsurface ice wedge structures do not extend to the surface and, as such, they do not relate to vegetation type, snow depth, or seasonal thaw depths changes across the transect.

4 CONCLUSIONS

Clear relationships are evident relating the subsurface, surface, and aerial imagery measurements at our three field sites. For example, the ice rich peat zone, with the tussock vegetation, is associated with the shallowest seasonal thaw depths and the deepest snow. The low lying tussocks and a lack of a dense vegetation canopy to intercept snow likely lead to the greater snow depths in thie area. In contrast, the mixed white spruce and birch forest had the deepest seasonal thaw, the shallowest snow depths, and the lowest ice content permafrost soils. The dense canopy in these areas likely intercepted more snow and led to lower snow depths. Similar ERT-surface-airborne imagery correlations between vegetation, ice content, and seasonal thaw were evident along the Creamer's Field transect. The Permafrost Tunnel site had a repeated ice wedge polygon pattern and no high ice content peaty soils. In addition, the vegetation composition did not change along the Permafrost Tunnel transect. As such, though the ERT values changed along the transect they did so at a small scale (5-10 m) and the spatial extent of our thaw depth and snow depth measurements was not fine enough to relate permafrost with these characteristics.

The relationships we found between ecotype, permafrost composition, and seasonal thaw dynamics could be used to apply biophysical characteristics and standoff measurements like aerial imagery, hyperspectral measurements, and LiDAR, to ascertain the presence or absence of permafrost in similar terrains. Clearly a more broad set of measurements and applications must be made before being able to scale our measurements elsewhere but these initial results are promising.

Our results also further confirm the application of ERT to map permafrost with clear relationships between frost probing, permafrost extent, and borehole cryostructural measurements.

ACKNOWLEDGEMENTS

This research was funded by the U.S. Army Corps of Engineers Engineer Research and Development Center's Center Directed Research Program, the U.S. Army Corps of Engineers Engineer Research and Development Center's 6.1 Basic Research Program, and the Department of Defense's Strategic Environmental Research and Development Program (Project RC-2110). We thank Amanda Barker, Maria Berkeland, Tiffany Gatesman, Stephanie Saari, Dana Brown, Art Gelvin and Malcolm Major for their help with field measurements. Merritt Turetsky helped develop the vegetation classifications. Hélène Genet assisted with development of the abstract in French (merci Hélène!).

REFERENCES

Chacho E., Arcone S., and Delaney, A. 1995. Blair Lakes target facility permafrost and groundwater study, *US Army Cold Regions Research and Engineering Laboratory*, Hanover, NH. 30 p.

Chapman, W.L., and Walsh, J.E. 2007. Simulations of Arctic temperature and pressure by global coupled models, *Journal of Climate*, 20(4): 609-632.

Douglas, T., Jorgenson, M.T., Kanevskiy, M., Romanovsky, et al. 2008. Permafrost dynamics at the Fairbanks Permafrost Experimental Station near Fairbanks, Alaska, *Proceedings of the Ninth International Conference on Permafrost*, edited by D. Kane, and K. Hinkel, pp. 373.

Douglas, T.A., Blum, J.D., Guo, L., Keller, K., and Gleason, J.D. 2013. Hydrogeochemistry of seasonal flow regimes in the Chena River, a subarctic watershed draining discontinuous permafrost in interior Alaska (USA), *Chemical Geology,* 335**,** 48-62.

Douglas, T.A., Jorgenson, M.T., Brown, D.R.N., Campbell, S.W., Hiemstra, C.A., Saari, S.P., Bjella, K., and Liljedahl, A.K. Degrading permafrost mapped with electrical resistivity tomography, airborne imagery and LiDAR, and seasonal thaw measurements. In press, *Geophysics*.

Grosse, G., Harden, J., Turetsky, M., McGuire, A.D., Camill, P., et al. 2011. Vulnerability of high-latitude soil organic carbon in North America to disturbance. *Journal of Geophysical research Biogeosciences,* 116(G4).

Hamilton, T.D., Craig, J.L. and Sellmann, P.V. 1988. The Fox permafrost tunnel: A late Quaternary geologic record in central Alaska, *Geological Society of America Bulletin,* 100(6): 948–969.

Harada, K., and Yoshikawa, K. 1996. Permafrost age and thickness near Adventfjorden, Spitsbergen, *Polar Geography,* 20, 4, 267-281.

Hauck, C., and Kneisel, C. 2008. *Applied geophysics in periglacial environments*. Cambridge: Cambridge University Press.

Hubbard, S.S., Gangodagamage, C., Dafflon, B., Wainwright, H., Peterson, J., Gusmeroli, A., Ulrich , C., Wu, Y., Wilson, C., Rowland, J., Tweedie, C., and Wullscheleger, S.D. 2013. Quantifying and relating land-surface and subsurface variability in permafrost environments using LiDAR and surface geophysical datasets, *Hydrogeology Journal*, 21, 1, 149-169.

Jorgenson, M., Osterkamp, T. 2005. Response of boreal ecosystems to varying modes of permafrost degradation, *Canadian Journal of Forestry Research,* 35(9): 2100–2111.

Jorgenson, M.T., Yoshikawa, K., Kanevskiy, M., Shur, Y., Romanovsky, V., et al. 2008, Permafrost characteristics of Alaska, *Proceedings of the Ninth International Conference on Permafrost*, edited by D. Kane, and K. Hinkel.

Kneisel, C. 2006. Assessment of subsurface lithology in mountain environments using 2D resistivity imaging, *Geomorphology,* 80(1): 32-44.

Lewkowicz, A.G., Etzelmüller, B., and Smith, S.L. 2011. Characteristics of discontinuous permafrost based on ground temperature measurements and electrical resistivity tomography, southern Yukon, Canada, *Permafrost and Periglacial Processes*, 22, 4, 320-342.

Loke, M.H., Acworth, I. and Dahlin, T. 2003. A comparison of smooth and blocky inversion methods in 2D electrical imaging surveys, *Exploration Geophysics*, 34, 182-187.

Mackelprang, R., Waldrop, M.P., DeAngelis, K.M., David, M.M., Chavarria, K.L., Blazewicz, S.J., Rubin, E.M., and Jansoon, J.K. 2011. Metagenomic analysis of a permafrost microbial community reveals a rapid response to thaw, *Nature*, 480: 368-371.

Myers-Smith, I., Harden, J., Wilmking, M., Fuller, C., McGuire, A, et al. 2008. Wetland succession in a permafrost collapse: interactions between fire and thermokarst, *Biogeosciences,* 5(5).

Nicholas, J.R., Hinkel, K.M. 1996. Concurrent permafrost aggradation and degradation induced by forest clearing, central Alaska, USA, *Arctic, Antarctic, and Alpine Research,* 28.

Osterkamp, T., Romanovsky, V. 1999. Evidence for warming and thawing of discontinuous permafrost in Alaska, *Permafrost and Periglacial Processes,* 10(1): 17–37.

Racine, C.H., Walters, J.C. 1994. Groundwater-discharge fens in the Tanana Lowlands, Interior Alaska, U.S.A., *Arctic and Alpine Research*, 26(4): 418-426.

Shur, Y. Jorgenson, M. 2007. Patterns of permafrost formation and degradation in relation to climate and ecosystems, *Permafrost and Periglacial Processes* 18(1): 7–19.

Smith, L.C., Sheng, Y., MacDonald, G.M., Hinzman, L.D. 2005. Disappearing Arctic lakes, *Science*, 308(5727): 1429-1429.

Sturm, M., Douglas, T.A. Racine, C. and Liston, G.E. 2005. Changing snow and shrub conditions affect albedo with global implications, *Journal of Geophysical Research Biogeosciences*, 110, G01004: doi:10.1029/2005JG000013.

Tarnocai, C. Canadell, J., Schuur E., Kuhry, P., Mazhitova, G., et al. 2009. Soil organic carbon pools in the northern circumpolar permafrost region, *Global Biogeochemical Cycles,* 23(2).

Walker, M.D., et al. 2006. Plant community responses to experimental warming across the tundra biome. *Proceedings of the U.S. National Academies of Science*, 103: 1342-1346.

Wilhelm, R.C., Niederberger, T.D., Greer, C., Whyte, L.G. 2011. Microbial diversity of active layer and permafrost in an acidic wetland from the Canadian High Arctic, *Canadian Journal of Microbiology*, 57: 303-315.

Wolken, J.M., et al. (2011) Evidence and implications of recent and projected climate change in Alaska's forest ecosystems, *Ecosphere*, 2(11): 1-35.

Yoshikawa, K., Leuschen, C., Ikeda, A., Harada, K., Gogineni, P., Hoekstra, P., Hinzman, L., Sawada, Y., and Matsuoka, N. 2006. Comparison of geophysical investigations for detection of massive ground ice (pingo ice), *Journal of Geophysical Research: Planets* (1991–2012), 111 E6, 10 pages.

Zimov, S.A., Schuur, E.A., Chapin, III, F.S. 2006. Permafrost and the global carbon budget, *Science,* 312(5780): 1612–1613.